Structural Behaviour of Supported Tubular Bus Structure in Substations under Seismic Loading

Structural Behavior of Supported Tubular Bus Structure in Substations under Seismic Loading

Qilin Sun[1,2], Guanglin Yuan[1], Yuner Huang*[3],Qianjin Shu[1], Qingtao Li[1]

[1] State Key Laboratory for Geomechanics & Deep Underground Engineering; School of Mechanics and Civil Engineering, China University of Mining and Technology, Xuzhou, Jiangsu 221116, China.
[2] School of City & Architecture Engineering, Zaozhuang University, Zaozhuang, Shandong 200160, China.
[3] Institute for Infrastructure and Environment, School of Engineering, The University of Edinburgh, Edinburgh, Scotland, UK.

Abstract

This paper presents an experimental investigation on structural behavior of a temperature member used to interconnect the supported tubular bus structure of 220 kV substation, and the dynamic interaction between the components of a bus insulator substructure under seismic loading. Finite element (FE) analysis was performed to analyze the seismic stress of the supported tubular bus structure. The results of quasi-static experiments showed an elastic deformation characteristic, while the temperature member exhibited a damping ratio of 4 - 7%, and elastic stiffness of 13.4 N/mm. Compared with the stand-alone configuration, the peak accelerations of insulators connected to the tubular bus through the temperature member were reduced by 10 - 30%, while the maximum displacements were reduced by 30%. The maximum displacement responses of insulators connected to the tubular bus through clips were roughly the same as those under the stand-alone configuration, while the peak accelerations were reduced by 30 - 50%. When the ground acceleration reached the value of 6.2 m/s^2, the root stress exceeded the yield strength of the material. Under this condition the insulators may experience fracture or collapse.

Keywords: Supported tubular bus, Post insulator, Seismic behavior, Seismic safety, Shake table tests, Quasi-static tests

* Corresponding author. Tel.: +44 (0) 131 650 5736; Fax: +44 (0) 131 650 6554.
E-mail address: Yuner.Huang@ed.ac.uk

1 Introduction

Tubular bus is a type of conductor connection commonly used on 220 kV substations, and is characterized by advantages of land-saving and convenient construction. Tubular bus is usually supported by a tall and slender insulator post. It is prone to damage under seismic activity, with most of the damages being the fracture of insulator post (Iwatsubo, 1998; Krishnamurthy et al., 2016). For instance, a substation in Deyang (China) experienced rupture and collapse of the insulator post during Wenchuan earthquake. This was accompanied by the falling-off of bus and other forms of damages, and all of it happened when the ground acceleration was as small as 1.36 m/s^2 (Eidinger, 2009). These damages break the connection between the substation and the power transmission system, eventually causing failure of the power system. In the Wenchuan earthquake, eleven substations failed to work properly because of this type of damage, which brought great inconvenience to relief and post-disaster reconstruction (Yu, 2008).

A flexible component is installed between the tubular bus and electrical equipment to adapt to the temperature-based deformation of bus, and reduce thermal stress of the structure. Previous researches have focused on investigating the deformation capacity, structural performance and design of the flexible component in substations. Filiatrault and Kremmidas (2000) conducted quasi-static tests to obtain force-displacement hysteresis loops of spring-type and sliding-type temperature members. Shaking table tests were conducted after installing the flexible members on a rigid wire-connected equivalent steel column system. It is shown that the spring-type temperature member increased the acceleration and displacement response of the steel column, while the sliding-type temperature member decreased its peak response. Stearns and Filiatrault (2004) designed a novel flexible connecting component, and performed both the quasi-static tests and the shaking table tests. Such a novel expansion component was characterized by a high damping ratio and high energy consumption, and could reduce the peak acceleration response of the equipment. Song and Der Kiureghian (2006a) put forward an asymmetric Bouc-Wen model to describe the constitutive relations of temperature members proposed in previous studies (Filiatrault and Kremmidas, 2000; Stearns and Filiatrault 2004), and defined the parameter range for the model.

In addition to flexible components, literature on rigid bus-connected equipment is reviewed in this paragraph. Song and Der Kiureghian (2006b) established a preliminary method for calculating the seismic response of rigid wire-connected equipment using the single degree of freedom (SDOF) model. In their work, the electrical equipment suffered restoring and damping forces caused by the rigid bus. Cheng et al. (2014) conducted shaking table tests to obtain the seismic coupling effect between the 1,000-kV lightning arrester and the transformer connected through rigid tubular bus, and reported that the damping effect of sliding hardware weakened the acceleration response of high-frequency equipment in this system. Günay et al. (2015) presented real-time hybrid simulation (RTHS) in shake table tests for testing a sub-structure in a substation. Alessandri et al. (2015) described the design and characterization of a base isolation system, which protected the ceramic circuit breakers during seismic events. Preliminary numerical analyses and tests were performed on a typical high voltage (HV) circuit breaker and demonstrated the decrease in bending moment in the isolation system during seismic activity. However excessive displacements of the electrical connecting cable in the latter can cause electrical insulation problems. Cheng et al. (2016) then carried out ground motion simulation tests on a rigid bus-connected 500 kV lightning arrester and a transformer, and found that the seismic coupling effect between the connected equipment increased with the increase in intensity. It improves the mobility of the sliding hardware.

In short, existing studies mainly focused on the structural performance of a temperature member, and its influence on the dynamic response of the equipment. Furthermore, the existing ground motion simulation experiments were all based on single-span structures. The research on complex systems, which contain multiple electrical equipments connected through buses, is scarce in literature. The existing theoretical models use SDOF model to represent the electrical equipment, and study the influence of bus as the spring restoring and damping forces. As a result, the coupling effect of seismic response between the tubular bus and the insulator post is ignored. As far as the structure of supported tubular bus is concerned, there is a lack of availability of data on the shaking table tests. Due to this reason, this paper mainly focuses on

studying the structure behavior of a supported tubular bus of a typical 220 kV substation. The results obtained in this paper can ascertain the structure behavior of a tubular bus under seismic activity, and improve the design guidelines of tubular bus structure. The conclusions will be used to increase the resilience of substations under seismic activities. The present work was conducted keeping in view the following objectives:

(1) Conduct quasi-static tests to determine the structure behavior of temperature members under cyclic loading, and calculate the damping ratio based on experimental data.

(2) Conduct ground motion simulation experiments to examine the influence of tubular bus and temperature member on the seismic performance of an insulator post.

(3) Perform finite element (FE) analysis to investigate the safety of supported tubular bus structure under earthquakes of different intensities.

2 **Deformation capacity of the temperature member**

Installed at the top of the insulator, the temperature member is used to fix the tubular bus on both sides, and has a certain deformation capacity. According to the results reported in previous studies (Filiatrault and Kremmidas, 2000; Stearns and Filiatrault 2004), the deformation capacity and the damping ratio of the temperature member influence the degree of dynamic coupling of the equipment. Therefore, in this section, the mechanical deformation and damping ratio of the temperature member have been studied under the influence of cyclic load using quasi-static tests. Furthermore, the results provide the basis of analysis and calculation parameters for the shaking table tests and FE simulation.

2.1 **Overview of the test**

An experimental investigation for the MGGD-130WP temperature member, which is commonly used in 220kV substation, is presented in this section. Each specimen was 460 mm in length, while two fasteners were connected using four aluminum stranded conductors, as shown in Figure 1(a). The temperature member is horizontally placed before the testing, with one end rigidly connected to the reaction wall through cantilever support, and the other end connected to the actuator through sliding support, as shown

in Figure 1(b). The bearing was installed at the bottom using a pulley, which can move horizontally. During the tests, the cyclic load was applied on the temperature member through the actuator. The actuator in the structural laboratory of China University of Mining and Technology (CUMT) was used for loading cycles. The actuator had a maximum force of 10 kN and a maximum displacement of 20 mm. The measurement of displacement-time data was realized using YHD-200 displacement meter, which logged all the data in a computer using Dh3818-1 data logger.

[insert Figure 1.]

2.2 Test loading mechanism

According to the Chinese standard (JGJ 101, 2015), a displacement-controlled loading system was adopted to apply cyclic loading on the temperature members. The loading protocol is shown in Figure 2. First, a compressive force was applied on the temperature member at the loading rate of 1 mm/min until the displacement reached 10 mm. Then tensile force was applied on the temperature member with the rate of 1 mm/min to the same displacement. Such a loading cycle was repeated 3 thrice. Further loading was applied with the displacements of 20, 30 and 40 mm in both the compression and tension tests, with each loading cycle repeated 3 thrice (as shown in Figure 2). After the temperature member reached its compressive limit at the displacement of 40 mm, tensile force was applied on the temperature member at the same rate for each loading cycle.

[insert Figure 2.]

2.3 Data analysis

The data obtained from the tests are reorganized into a hysteresis loop, which shows the relationship between tractive force and displacement (Figure 3(a)). In the direction of compression, the displacement was increased until the contact between the two fasteners occurred. In the tensile direction, the displacement was increased with deformation of the four aluminum stranded conductors. The behavior of the temperature member was similar to the rigid bus slide (Song and Der Kiureghian, 2006), which represents a typical Coulomb friction coupled with an elastic restoring force mechanism.

On the hysteresis loop, the maximum load of each loading cycle in the same direction (tensioning or compressing) was connected to obtain a smooth curve (Figure 3(c)). On this curve, the tensile and compressive intervals were approximated as parabolas. According to the behavior of specimens (shown in Figure 3(b)), the elastic stiffness can be estimated to be 13.4 N/mm. When the displacement was less than 40mm, the curve was almost a skewed line, indicating that the deformation of the temperature member lies within an elastic period at this point. When the displacement reached 40 mm, the curve showed an inflection point and became less steep, suggesting that the rigidity of the temperature member began to degrade from this point on. The smooth curve did not show any declining phase, suggesting that the temperature member has not reached its ultimate bearing capacity within its deformation capacity.

The force-displacement hysteresis loop area formed after each level of loading/unloading represents the energy dissipated by the temperature member during the process of deformation. The deformation energy is introduced to calculate the damping ratio of the temperature member under each loading cycle. According to previous studies (Filiatrault and Kremmidas, 2000), the damping ratio ζ can be given by Eq (1),

$$\zeta = \frac{E_{D\delta}}{2\pi F_{\delta}\delta} \tag{1}$$

where the parameters δ, $E_{D\delta}$ and F_{δ} represent the maximum displacement, the deformation energy, and the ultimate force in each loading cycle, respectively. The results of the damping ratio of temperature section under each level are shown in Figure 3(d).

The damping ratio of the temperature member ranged between 4 - 7%, which is 25 - 50% of the damping ratio of a rigid bus slide described in literature (Filiatrault and Kremmidas, 2000). In the temperature member, the deformation of aluminum strands provided all the capability to dissipate energy, while the rigid bus slide existing inside and outside the sleeve friction can dissipate extra energy. This results in the difference of damping ratio between the two. According to Stearns and Filiatrault (2004), the connection component having high damping ratio and high energy consumption could

reduce the peak acceleration response of the equipment. Therefore, further research should be conducted to increase the damping ratio of the temperature member to keep the electrical equipment safe during seismic activity.

[insert Figure 3.]

3 Ground Motion Simulation Test for the structure of Tubular Bus

3.1 Test Specimen and Setup

The structure of a typical 220 kV supported tubular bus has the length and height of 78 m and 9 m, respectively. It is impossible to conduct a full-scale ground motion simulation test due to the limited capacity of shaking table. According to some specifications (GB 50260, 2013; IEEE693, 2015), when it is impossible to conduct full-scale structural shaking table tests on an equipment set, the equipment can be broken down into sub-assemblies which are tested separately. Mosalam et al. (2012) compared the test results of substructures and the full-scale structure using shaking table tests, and showed that the difference of dynamic characteristics between the two was less than 10% when the dynamic amplification factor was taken into account. Moustafa et al. (2016) also followed this principle in conducting a substructure shaking table test on disconnectors.

Therefore, the insulator post, which is a part of the structure connecting the tubular bus, has been selected in this work as the test structure (Figure 4(a)). The influence of both the tubular bus and the temperature member on the dynamic characteristics of the insulator post has been investigated. Three groups of insulators (Posts A, B and C) were connected to the tubular bus to constitute a two-span structure, as shown in Figure 4. Posts A and C were connected to the tubular bus using fixed supports, while Post B was connected to the tubular bus using the temperature member. The distance between the insulators post was 2.6 m, while three balancing weights (each 30 kg in mass) were added to the tubular bus to compensate for the mass lost from the span shortening. Figure 4(b) shows that the Post D was not connected to the tubular bus, to compare its dynamic response with that of the other insulators. It can be used to measure the influence of tubular bus on the ground motion response of the insulator posts. The

insulators used in the test setup were ZSW3-252 outdoor rod-shaped posts, having a porcelain post body and a shed diameter of 245 mm. Each post consisted of two insulator porcelain bottles connected through six steel bolts of 18 mm in diameter. Each porcelain bottle was 1.1 m in height, and its bottom was connected to the steel bearing through eight steel bolts of 18 mm in diameter. The steel bearings were linked to the shaking table board using four anchor rods, which ensured that there was no sliding between them during the test. Furthermore, the tubular bus had the inner and outer diameters of 0.24 m and 0.26 m, respectively.

[insert Figure 4.]

3.2 Layout of measuring points and test instruments

At its top, each post insulator was equipped with an acceleration sensor (A-1～A-4 in Figure 7) and a displacement sensor (U-1～U-4 in Figure 7) to obtain its maximum acceleration and displacement data. The shaking table in the structural laboratory of Southeast University (SEU), China was used to conduct the tests for the loading of ground motion simulation. The shaking table board had the dimensions of 4 m × 6 m, and had the maximum acceleration of 14.7 m/s^2 (horizontal). The acceleration-time data were collected using four CA-YD accelerometers, which logged the data in a computer. The measurement of displacement-time data was realized using two NR600 laser displacement meters and two AZ716 guyed displacement meters.

[insert Figure 5.]

3.3 Test procedure

Based on a previous study (Takhirov et al., 2005; Lam et al., 2016; Kaveh and Mahdavi, 2017) focusing on the experimental seismic wave of substation equipment, four earthquake ground motions are used for the seismic tests on the shake table: El-centro (1940 USA earthquake), Taft (1952 USA earthquake), Kobe (1995 Japan earthquake) and artificial seismic wave. Figure 6 shows the response spectrum curve with the damping ratio of 2% for all of the seismic waves.

[insert Figure 6.]

The first step of loading was run at a low acceleration (1 m/s^2). Then, the amplitude of each level's loading cycle was increased by 1 m/s^2. The peak acceleration of the

seismic ground motion was increased until the structure was damaged, or the capacity of the shaking table was exceeded. During the tests, the deformation of tubular bus or the collapse of the insulator post was not observed. Furthermore, the stripping slip at any flange position was not observed. The vibratory response of the tested structure was relatively insignificant when the peak acceleration of the applied seismic ground motion was less than 3 m/s^2. On the other hand, the tested structure showed obvious vibrations when the peak acceleration was increased to 4 m/s^2. The El-Centro seismic ground motion, the Taft seismic ground motion and the artificial wave were kept running until 5 m/s^2. The Kobe seismic wave worked until 9 m/s^2. After the completion of test, the aluminum stranded conductor of the temperature member showed no observed deformation.

3.4 Data analysis

3.4.1 Natural frequency data

White noise with the peak acceleration of 1 m/s^2 was input before the test and after the loading of each level to examine the change in natural frequency. The data of natural frequency of post D are shown in Figure 7.

[insert Figure 7.]

The results show that the natural frequencies before and after the test were 20.57 Hz and 19.4 Hz, respectively, indicating a rate of change of 9.8%. It shows that during the experiment, although there was no large deformation in the structure, internal damage still occurred to the structure, resulting in a decrease in the stiffness of the structure and a decrease in the natural frequency.

3.4.2 Acceleration-time data

The maximum response acceleration data of the insulator posts under the action of various seismic ground motions were acquired, and the results are shown in Figure 8.

[insert Figure 8.]

As shown in Figure 8, when the seismic action had the acceleration of 1 m/s^2, the peak accelerations of various insulator posts are similar to each other. With the increase in the acceleration of input seismic activity, the response accelerations of most of the insulator posts increased. Under the action of El-centro and Taft, the response

acceleration of Post D increased at the fastest pace. Its peak acceleration was about 1.5 times that of the peak accelerations of other posts under the working conditions of same level. Under the action of Kobe, the acceleration responses of Posts B and D were relatively similar to each other, and both increased relatively quickly. When the input seismic acceleration was less than 4 m/s^2, their acceleration responses were 1.5 times greater than those of Posts A and C. For the input seismic acceleration of 8 m/s^2, the acceleration responses were two times higher than those of the Posts A and C. Under the action of artificial seismic wave, the acceleration of Post B increased relatively quickly, while its numerical value was greater than those of the other insulator posts. In order to quantitatively analyze the influence of tubular buss and connection mode on the acceleration responses of the insulator posts, the acceleration amplification factor (AAF) was defined using Eq (2) (Filiatrault and Kremmidas, 2000):

$$AAF = \frac{a_c}{a_a} \tag{2}$$

where the parameters a_c and a_a are the maximum accelerations of the post with and without bus, respectively. The results calculated using Eq (2) are shown in Figure 9.

[insert Figure 9.]

As shown in Figure 9, under most of the circumstances, the AAF of various post insulators have value of less than 1, suggesting that the peak accelerations of insulators decreased after the addition of tubular bus. This is because the structural form of insulator posts changes from cantilever beam to frame column with top constraint after connecting the tubular bus, while the presence of a tubular bus increases the lateral rigidity of insulators and further reduces their acceleration responses. When the peak acceleration of the seismic wave was less than 4 m/s^2, the value of the AAF of various posts were relatively stable. This means that, under the action of El-Centro, they lied with the range of 0.4 - 0.7, whereas under the action of Taft, they lied with the range of 0.5 - 0.8. Similarly, under the action of Kobe, they had value of around 0.7. In addition, under the action of artificial wave, the acceleration influencing factors of Posts A and C lied with the range of 0.7 - 0.9, while that of Post B lied with the range of 1.0 - 1.2. When the peak value exceeded 4 m/s^2, with the increase of acceleration, the value of the

acceleration influencing factor of Post B gradually increased from 0.7 to 1.0. However, of the corresponding value of the Post A decreased from 0.5 to 0.3. This suggests that the deformation of temperature member gradually increased with the increase in the intensity of seismic activity. In addition, when the deformation of temperature member entered the rigidity degradation stage (see Figure 3(b)), the top constraint of insulators weakened, due to which, the differences between the peak accelerations of Post B and those of Posts A and C were enlarged.

3.4.3 Analysis of the displacement data

The limiting displacements of insulator posts under the action of seismic waves of different intensities are shown in Figure 10.

[insert Figure 10.]

The maximum displacements of insulator posts differed significantly under the action of various seismic waves, as shown in Figure 10. This means that the maximum displacements of the insulator posts under the action of El-centro and artificial seismic wave were 4 - 8 times greater than those under the action of Taft and Kobe. With the enhancement of seismic action, the response displacements of various posts increased proportionately, while the displacement responses of Posts A and C, which were rigidly connected to the tubular bus, were close to that of the Post D. Furthermore, the displacement of Post B connected with the tubular bus through the temperature member was 25 - 36% less than those of the other posts. In this study, a displacement amplification factor (DAF) is used to quantify the displacement of the tested structure, and is defined using Eq (3) (Filiatrault and Kremmidas, 2000).

$$DAF = \frac{d_c}{d_a} \tag{3}$$

where the parameters d_c and d_a are the maximum displacements of posts with and without the bus, respectively. The results calculated using Eq (3) are shown in Figure 11.

[insert Figure 11.]

The value of the DAF of various insulator posts were similar under various seismic waves, as shown in Figure 11. The value of the DAF for Posts A and C were about 1.0,

while that of Post B lied within the range of 0.6 - 0.8. This is because the insulators have an extremely high rigidity and an extremely low deformation. As a result, the peak displacements of Posts A, C and D were all close to the displacement of shaking table. However, the temperature member experienced a certain deformation in the tests, while its deformation restoring force limited the vibration of Post B and reduced its displacement.

4 Finite Element Analysis

4.1 Validation of the finite element model

ANSYS software was used to develop the finite element model for the structure shown in Figure 4(a) (hereinafter referred to as Model 1). In Model 1, Beam188 was adopted as the beam element to simulate the insulator post, the steel support and the aluminum tubular bus. The material properties of the components are provided by the manufacturer, and are listed in Table 1. Linear elastic material model was adopted to simulate the insulator porcelain, while bilinear isotropic model was used for aluminum tubes and steel supports. The contact between Post A/Post C and the tubular bus was defined as the fixed joint, which means, the elements of the insulator posts and the tubular bus in the joint shared a single node. In addition, Combin14 spring element was adopted to simulate the temperature member connecting the Post B and tubular bus. In the model, the restricted spring element moved and rotated in y and z directions. Only the deformability in x direction was retained. The elastic stiffness and the damping ratio of Combin14 spring element were 13.4N/mm and 5%, respectively, which were determined according to the procedure described in Section 2.3. The balancing weights were simplified as the mass points. The Model 1 is shown in Figure 12.

[insert Table 1.]

[insert Figure 12.]

The seismic ground motions used in the simulations were the same as those reported in Section 3.3. The results, along with the experimental data under the same intensity as reported in Section 3.4, are presented in Table 2. The calculated top acceleration-time data of the insulator posts were presented, and compared with the test

results in Figure 13. The numbers in brackets in Figure 13 represent the absolute values of the peak accelerations.

[insert Table 2.]

[insert Figure 13.]

The comparison of calculated and experimental results show that, the difference between the experimental and calculated results for Post B lied within the range of 2% - 11% under the El-centro, Taft, Kobe and the artificial wave of 3 m/s^2, while the difference was 29% under the artificial wave of 4 m/s^2. The experimental and calculated results agree well to each other. This means that it is reasonable and feasible to simplify the temperature members as a spring element. As indicated by the results presented in Table 2, the calculation results of peak acceleration on Post A were mostly larger than the experimental data, which suggests that the difference between them was higher than 20% under artificial wave of 3 m/s^2, while the difference lied within the range of 0 - 16% under the El-centro, Taft, Kobe and artificial wave of 4 m/s^2. The calculated results of Post C were all less than the corresponding experimental data, which suggests that the difference between them was higher than 20% under the El-centro and lied within the range of 0 - 14% under the artificial wave, Taft and Kobe. In Model 1, the configurations of Post A and Post C were the same as the construction and connection with bus that caused Post A and Post C to have the same performance in the seismic simulation. However, in the tested structure, the slide existing between the fixed support and the tubular bus resulted in the difference of experimental data between Post A and Post C. It is shown in Figure 13 that the acceleration-time curve obtained through calculations agrees well to that of the experimental data, and that the magnitudes of peak values coincided with the time of occurrence, suggesting that the finite element model is reasonable and accurate.

4.2 Finite element analysis of the seismic performance of supported tubular bus structure

4.2.1 Finite element model and application of seismic wave

A full supported tubular bus structure contains seven ∏-type steel supports, each of which has three sets of insulator at the top. Each set of insulators supports one tubular

bus (seen in Figure 14). According to the method described in Section 4.1, a finite element model for full-scale structure of the supported tubular bus was adopted to investigate the safety of supported tubular bus structure under different seismic intensities (hereinafter referred to as Model 2). In Model 2, the ∏-type steel support adopted Beam188 as the beam element for simulations, while the simulations of the insulator post and aluminum tubular bus were the same as those in Model 1. The material properties of these components are listed in Table 1. The simulation of the connection between the Post E/Post F and the tubular bus was the same as that of Post B in Model 1, while the simulation of Post G/Post H was the same as that of the Post A in Model 1. In addition, Post I and Post J were connected to the tubular bus through sliding hardware. The bus can slide in the hardware, thus only the displacements in *y* and *z* directions of the connection node between the insulator posts and the tubular bus were coupled. The model 2 is shown in Figure 14.

[insert Figure 14.]

The calculations were performed for the El-centro, the Taft and the artificial seismic waves. According to the seismic fortification intensity according to Chinese specification (GB 50260, 2013), the seismic fortification intensities of most of the regions in China range between Grades 6 and 8. Given that the substations are lifeline projects of vital significance for national economy, the seismic fortification intensity should be correspondingly elevated by one grade. Therefore, three seismic intensities were used, namely the Grade 7 rare earthquake having the maximum acceleration of 2.2 m/s^2, Grade 8 rare earthquake, having the maximum acceleration of 4 m/s^2 and Grade 9 rare earthquake having the maximum acceleration of 6.2 m/s^2. Considering that the insulator posts were longitudinally connected at the top using tubular bus and transversely linked at the bottom using supporting steel beam, the directions of the actions of two seismic waves were determined (in *x* and *z* directions).

4.2.2 Model Analysis

Model analysis of supported tubular bus structure was conducted to determine the natural frequencies and mode shapes of the entire structure. In ANSYS, the subspace method can be used to calculate the natural frequencies and mode shapes. The shapes of

the first 6 modes are presented in Figure 15. The numbers in brackets in Figure 15 represent the values of the natural frequencies.

[insert Figure 15.]

The first four modes correspond to the motion in X direction, while the last two modes correspond to the motion in Z direction. The fundamental periods of 0.931 s and 0.880 s mainly correspond to the deformation occurred on all of the tubular buses and ∏-type supports. On the contrary, the fundamental period of 0.719 s and 0.613 s correspond to the deformation just occurred on the tubular buses and ∏-type support in one end.

4.2.3 Influence of the Support

The conclusion based on a previous study (Mosalam et al. 2012, Moustafa et al. 2016) has shown that the dynamic characteristics of the insulator posts can be changed by steel frame installed on the bottom of these insulator posts. The results of acceleration of the insulator posts in Model 2 under seismic activity in X direction, along with the data under the same intensity as reported in Section 4.1, are presented in Table 3. The location of insulator posts are given in Figure 12 and Figure 14.

[insert Table 3.]

According to the data shown in table 3, the acceleration of posts in Model 2 are all higher than the value of post in Model 1, which indicated that the support improved the dynamic response of the insulator posts under seismic activity. The amplification between the results of Model 2 and Model 1 for the Post, which had same method connected with bus, lied within the range of 1.1 - 1.2 under the Taft, while the amplification lied within the range of 1.5 - 1.6 under the Kobe and 1 – 1.2 under artificial wave. Under the El-centro, the acceleration of Post G/Post H were 1.4 -1.5 times than the value of Post A, while the amplification lied within the range of 1.03 - 1.1 between Post E/Post F and Post B.

4.2.4 Analysis of the stress data

As indicated by the calculated results, the maximum moments of insulator posts occurred at the connection with the ∏-type support at the bottom. The principal stress of the insulator posts under the action of various seismic waves is provided in Table 4.

[insert Table 4.]

As indicated by the data presented in Table 4, under the action of seismic ground motions applied in the *z* direction, the root stresses of insulators at the same position were 3 - 7 times greater than those under the action of seismic wave applied in the *x* direction. It is clear from the comparison data (see Table 4.) that, when the seismic wave was applied in the *x* direction, the stresses of Posts E and F connected through temperature member were greater than those of the permanently connected Posts G and H. However, they were all smaller than those of Posts I and J having the slip connection. When the seismic wave was applied in the *z* direction, the Post I exhibited the highest stress. According to a previous study (GB 50260, 2013), when the stress values were adopted to calculate the indices of structural seismic strengths, the yield strength of insulator posts was 12.67 MPa. By comparing it with the data presented in Table 4, it can be seen that, when the peak acceleration of the input seismic ground motion reached 2.2 m/s^2, the stresses of various insulators were all lower than the allowable stress, due to which, there will be no failure. This means that, when the peak acceleration of the input seismic ground motion reached 4 m/s^2, Post I approached the limiting value, while the insulators achieved the critical state. Therefore, when the peak acceleration of the input seismic ground motion reached 6.2 m/s^2, the stresses applied on most of the posts exceeded the allowable stress of the structure, due to which, the supported tubular bus structure may become dangerous.

5 Conclusions

This paper presents an experimental and numerical investigation on the supported tubular bus structure of 220 kV substations. Quasi-static tests on a temperature member and shaking table tests on a two-span tubular bus insulator substructure were conducted. Finite element analysis was performed to examine the seismic stress of the supported tubular bus structure. Based upon the results, following conclusions are drawn.

(1) The constitutive relations of the temperature member used on the supported tubular bus structure of 220 kV substations manifested an elastic deformation characteristic, while the structural member exhibited a damping ratio of 4 - 7% (5% for

the finite element model).

(2) The seismic responses of insulator posts after the addition of a tubular bus were weakened, and their peak accelerations were reduced by 10 - 50%.

(3) The peak accelerations of the insulators connected to the bus through temperature member were 10% larger than those of the rigidly connected insulators.

(4) The maximum displacement responses of the insulators connected to the tubular bus through clips were roughly the same as those under the stand-alone configuration, and they were all 30% greater than those of the insulators connected through the temperature member.

(5) When subjected to seismic activity in the axial direction of the bus, the insulators experienced the bi-axial bending or combined bending-torsional stress. When subjected to seismic activity vertical to the axial direction of the bus, the insulators experienced the uniaxial bending, in which case the structural member was subjected to a higher stress. When the ground acceleration reached 6.2 m/s^2, the root stress exceeded the allowable stress of the material, and the insulators may experience fracture or collapse, thus placing the supported tubular bus structure in a dangerous state.

The results obtained in this paper can be applied to seismic design and seismic safety assessment for the supported tubular bus structure of 220 kV substations, and are also of significant value for the design of other types of substations. In this regard, the assessment of the seismic safety of insulators, the changes of acceleration response and displacement response of insulators under seismic activity caused by the bus and the connection methods should be considered. Under different connections, the stress of the insulators varies greatly, and therefore, it is necessary to enhance the strength of the insulator posts when carrying out seismic design.

Acknowledgements

This research was supported by Doctoral Program of Higher Education of China (201 6M601911), Natural Science Foundation of Jiangsu Province (BK20170282), Science and Technology Development Program of Zaozhuang (2016GX33).

References

Alessandri S, Giannini R, Paolacci F, Amoretti M, Freddo A. (2015) "Seismic Retrofitting of an HV Circuit Breaker Using Base Isolation with Wire Ropes Part 1: Preliminary Tests and Analyses". *Engineering Structures*, 98: 251–262

Cheng Y-F, and Qiu N. (2014) "Shake Table Test on Seismic Performance of 1000 kV Arrester and Capacitor Voltage Transformer Interconnected by Tube Bus". *High Voltage Engineering*, 40(12): 3882-3887.

Cheng Y-F, Zhu Z-B, Lu Z-C, Li S, Qiu N, Zhong M. (2016) "Earthquake Simulation Shaking Table Test on Coupling System of 500 kV Surge Arrester and Instrument Transformer Interconnected With Rigid Tube Bus". *Power System Technology*, 40(12): 3945-3950

China Power Engineering Consulting Group Northwest Electric Power Design Institute (2013), Code for Seismic Design of Electric Power Facilities, (GB 50260:2013), Standards China, Beijing.

Eidinger J (2009) "Wenchuan Earthquake Impact to Power Systems". *Lifeline Earthquake Engineering in a Multihazard Environment.* Technical Council on Lifeline Earthquake Engineering Conference (TCLEE) 2009. Oakland, California, US. pp. 1359-1370.

Filiatrault A, and Kremmidas S (2000) "Seismic Interaction of Interconnection Electrical Substation Equipment". *Journal of Engineering Mechanics*. 126(10): 1140-1149.

Günay S, Mosalam K, Takhirov S. (2015), "Real-time Hybrid Simulation in a Shaking Table Configuration for Parametric Studies of High-voltage Equipment and IEEE693 Development". *Nuclear Engineering and Design*. 295: 901-909

Housing and Urban-Rural Development (2015), Code for Seismic Test of Buildings, (JGJ 101:2015), Standards China, Beijing.

Institute of Electrical and Electronics Engineers (2015), IEEE Standard for Recommended Practice for Seismic Design of Substations, (IEEE 693:2015), IEEE, New York.

Iwatsubo T (1998) "Damage to Industrial Equipment in the 1995 Hyogoken–Nanbu Earthquake". *Nuclear Engineering and Design*. 181(1-3): 41–53.

Kaveh A. and Mahdavi V R. (2017) “Modification of Ground Motions Using Wavelet Transform and VPS Algorithm”. *Earthquakes and Structures*. 12(4): 389-395

Krishnamurthy V, Kwasinski A, Dueñas-Osorio L. (2016) “Comparison of Power and Telecommunications Dependencies and Interdependencies in the 2011 Tohoku and 2010 Maule Earthquakes”. *Journal of infrastructure System.* 22(3): 1-16.

Lam N, Tsang H-H, Lumantarna E. (2016), “Minimum Loading Requirements for Areas of Low Seismicity”. *Earthquakes and Structures*. 11(4): 539-561

Mosalam K M, Moustafa M A, Günay S, Triki I, Takhirov S. (2012) “Seismic Performance of Substation Post Insulators for Vertical-break Disconnect Switches”. California Energy Commission. *Report No.: CEC-500-2012*.

Moustafa M A, and Mosalam K M (2016) “Structure Performance of Porcelain and Polymer Post Insulators in High Voltage Electrical Switches”. *Journal of Performance of Constructed Facilities*. 30(5): 1-11

Stearns C, and Filiatrault A (2004) “Electrical Substation Equipment Interaction—Experimental Rigid Conductor Studies”. Structural Systems Research Project, *Report No. SSRP-2003/11*, University of California, San Diego.

Song J, and Der Kiureghian A (2006a) “Generalized Bouc-Wen Model for Highly Asymmetric Hysteresis”. *Journal of Engineering Mechanics*. 132(6): 610-618.

Song J, Der Kiureghian A, Sackman J L. (2006b) “Seismic Response and Reliability of Electrical Substation Equipment and Systems”. *Peer Report 2005/15*, Pacific Earthquake Engineering Research Center, University of California, Berkeley.

Takhirov S M, Fenves G L, Fujisaki E, Clyde D. (2005) “Ground Motions for Earthquake Simulator Qualification of Electrical Substation Equipment”. *Peer Report 2004/07*, Pacific Earthquake Engineering Research Center, University of California, Berkeley.

Yu Y-Q, Li G-F, Li P, Zhu Q-J, Yuan D-L, Wang C-Y, Li J-Z, Huang H, Li L-X, Zhang X-H, Liu J-M. (2008) “Investigation and Analysis of Electric Equipment Damage in Sichuan Power Grid Caused by Wenchuan Earthquake”. *Power System Technology*. 32(11): T1-T6.

Tables list

Table 1. Material Properties of Supported Tubular Bus

Structural Components	Support	Tubular Bus	Post Insulator
Material Types	Steel	Aluminum Alloy	Ceramic
Poisson Ratio	0.3	0.5	0.32
Elastic Modulus(GPa)	210	71.7	76.5
Density(Kg/m^3)	7800	2700	4600
Tangent Modulus at Yield Strength(GPa)	2	0.5	-
Yield Strength (MPa)	400	175	-

Table 2. Peak Accelerations of Post from Tests and Analysis

Levels of Seismic Waves	Type of Seismic Waves	Peak Accelerations of Post								
		Post A			Post B			Post C		
		Analysis (m/s^2)	Tests (m/s^2)	Analysis / Tests	Analysis (m/s^2)	Tests (m/s^2)	Analysis / Tests	Analysis (m/s^2)	Tests (m/s^2)	Analysis / Tests
3m/s²	El Centro	4.9	5.8	0.84	6.8	7.1	0.96	4.9	6.8	0.72
	Taft	6.4	6.2	1.03	7.2	6.5	1.11	6.4	6.5	0.98
	Kobe	5.6	4.9	1.14	5.5	6.0	0.92	5.6	5.8	0.97
	Artificial Wave	5.6	4.5	1.24	7.4	7.6	0.97	5.6	5.6	1.00
4m/s²	El Centro	6.2	6.2	1.00	9.2	9.0	1.02	6.2	7.9	0.78
	Taft	8.1	7.6	1.07	9.4	8.7	1.08	8.1	8.2	0.99
	Kobe	6.3	6.2	1.02	7.0	7.4	0.95	5.9	6.8	0.87
	Artificial Wave	6.7	6.2	1.08	9.8	13.8	0.71	6.7	7.1	0.94

Table 3. Peak Accelerations of Post from Model 1 and Model 2（m/s^2）

Type of Seismic Waves	Post A (m/s^2)	Post G (m/s^2)	Post H (m/s^2)	Post G/ Post A	Post H/ Post A	Post B (m/s^2)	Post E (m/s^2)	Post F (m/s^2)	Post E/ Post B	Post F/ Post B
El Centro	6.2	8.8	9.43	1.42	1.52	9.2	9.52	9.88	1.03	1.07
Taft	8.1	9.37	9.56	1.16	1.18	9.4	11.4	11.1	1.21	1.18
Kobe	6.3	8.94	9.58	1.42	1.52	7	10.94	11.59	1.56	1.66
Artificial Wave	6.7	7.81	7.84	1.17	1.17	9.8	11.34	9.2	1.16	0.94

Table 4. Principal Stress of Post Insulators (MPa)

Seismic Waves and Direction	Peak Acceleration	Location of Posts					
		E	F	G	H	I	J
El centro *x* Direction	2.2m/s^2	0.65	0.26	0.64	0.09	3.59	2.08
	4m/s^2	1.09	0.44	1.03	0.14	5.87	3.42
	6.2m/s^2	1.83	0.74	1.80	0.25	10.11	5.87
Taft *x* Direction	2.2m/s^2	0.57	0.26	0.50	0.07	2.64	1.59
	4m/s^2	1.03	0.47	0.92	0.13	4.80	2.89
	6.2m/s^2	1.60	0.74	1.42	0.20	7.45	4.48
Artificial seismic Wave *x* Direction	2.2m/s^2	0.70	0.27	0.67	0.09	3.74	2.20
	4m/s^2	1.19	0.48	1.17	0.16	6.47	3.80
	6.2m/s^2	1.97	0.77	1.89	0.27	10.53	6.19
El centro *z* Direction	2.2m/s^2	3.52	3.05	4.89	4.23	6.67	4.83
	4m/s^2	5.73	4.76	8.03	6.67	10.99	7.49
	6.2m/s^2	9.92	8.59	13.78	11.92	18.81	13.60
Taft *z* Direction	2.2m/s^2	3.01	2.24	4.16	3.04	4.97	3.23
	4m/s^2	5.47	4.08	7.56	5.53	9.04	5.88
	6.2m/s^2	8.48	6.32	11.72	8.58	14.01	9.11
Artificial seismic Wave *z* Direction	2.2m/s^2	3.93	2.99	5.52	4.30	6.98	4.72
	4m/s^2	6.72	5.24	9.39	7.49	12.00	8.27
	6.2m/s^2	11.07	8.43	15.55	12.12	19.67	13.29

Figures list

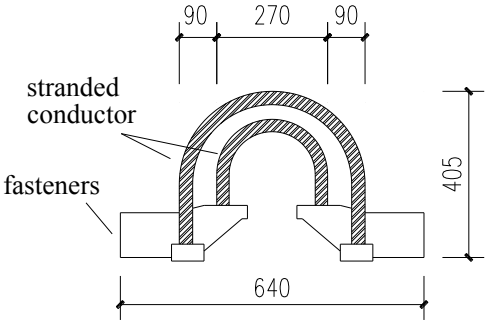

(a)Details of temperature members

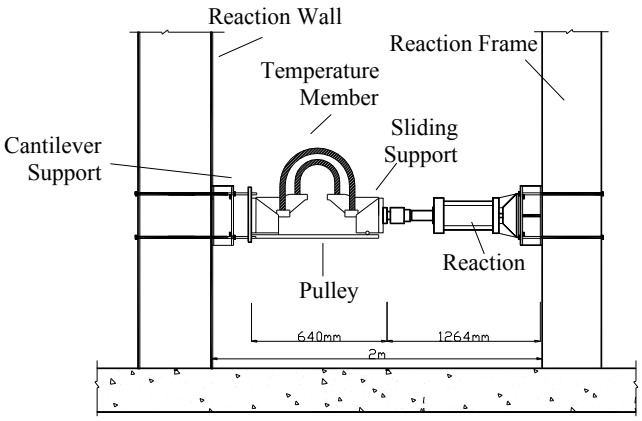

(b)Schematic test setup

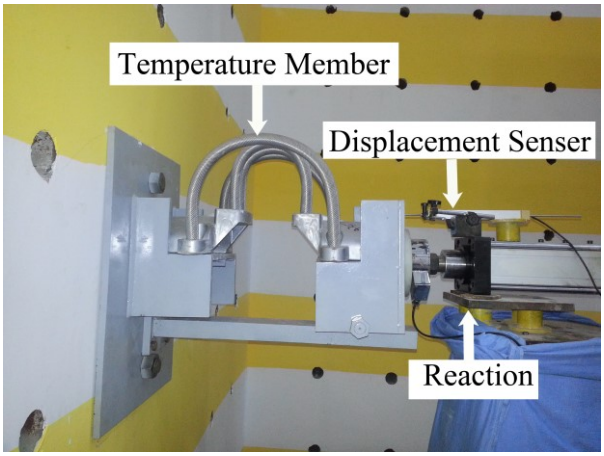

(C) General View

Figure 1. Experimental Setup

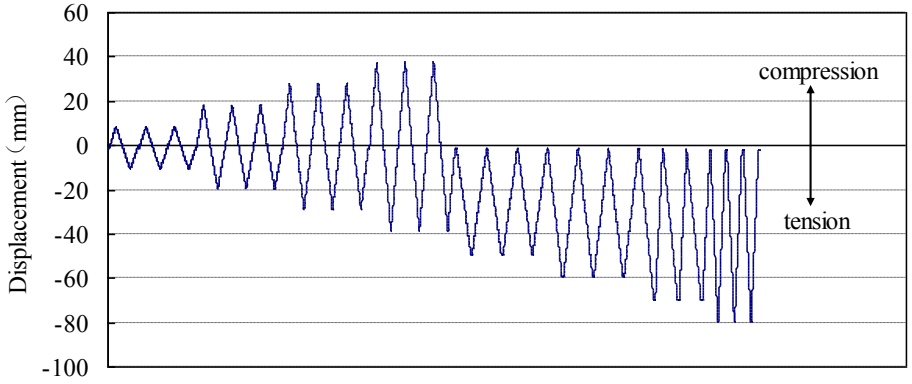

Figure 2. Loading Protocol

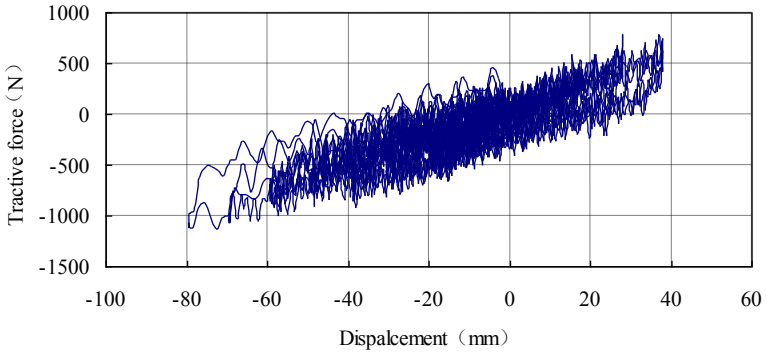

(a)Load-Displacement Responses of Temperature Member

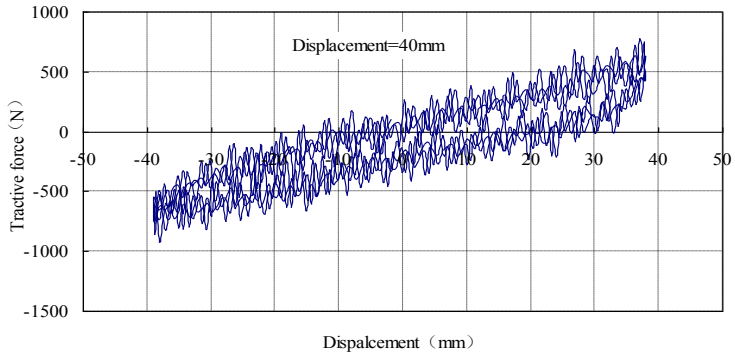

(b) Hysteresis loop on 40mm

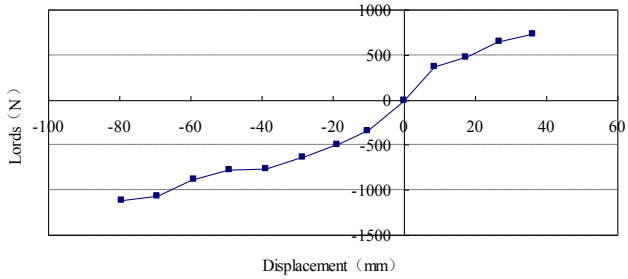

(c)Skeleton Curve

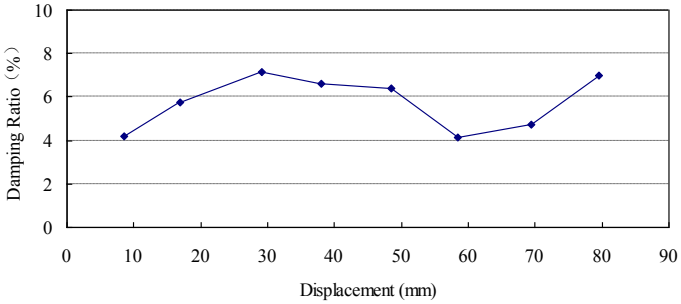

(d) Damping Ratio-displacement responses

Figure 3. Mechanical Properties of Temperature Member

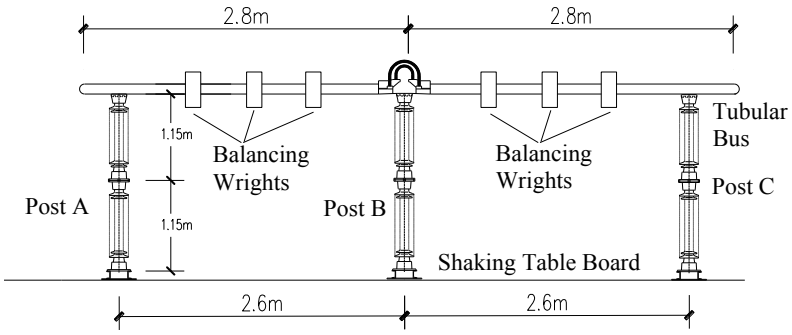

(a)Schematic test setup

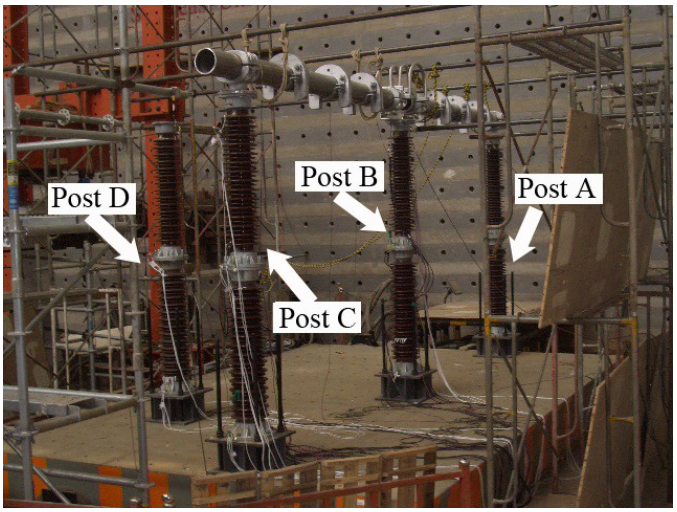

(b)General View on Shake Table

Figure 4. Test Structure

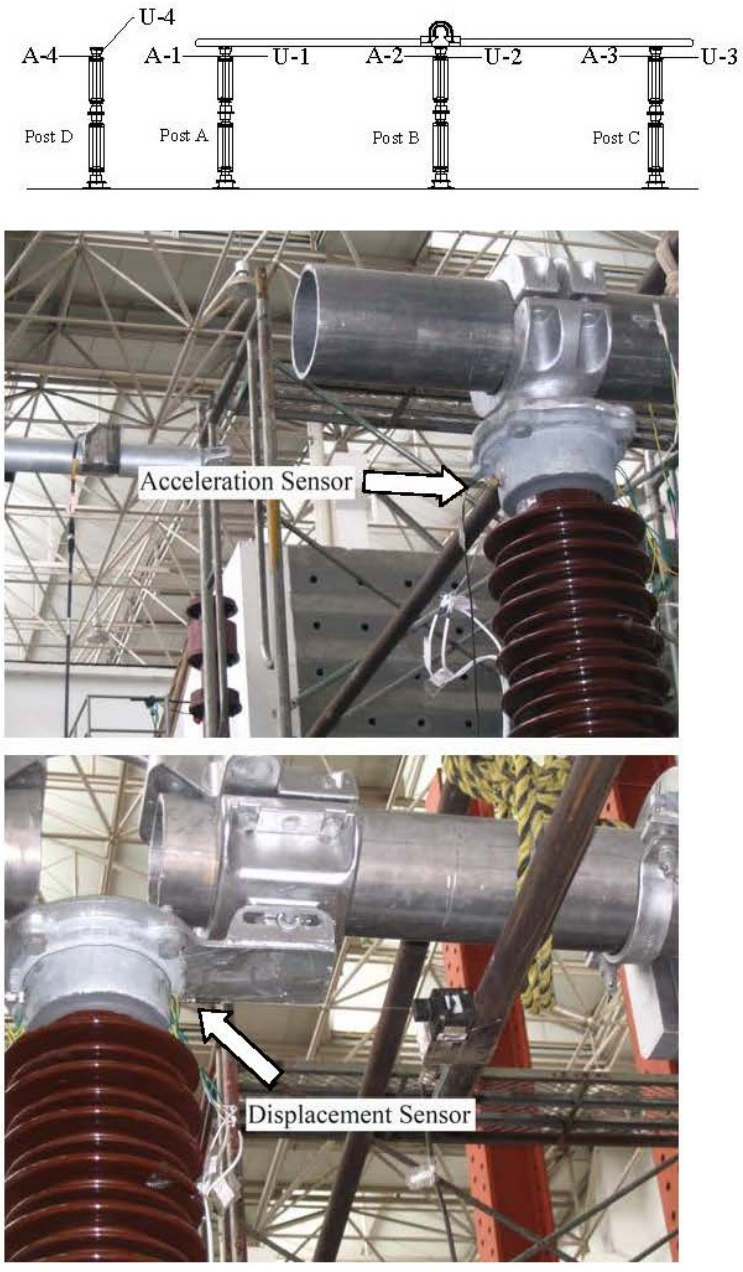

Figure 5. Arrangement of Sensors and details

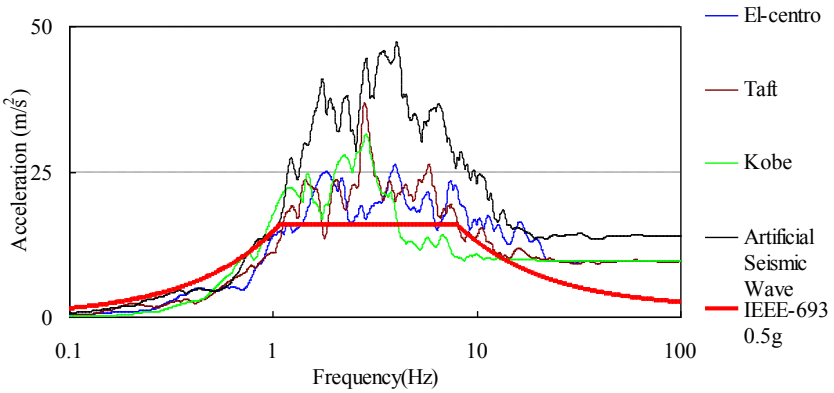

Figure 6. Acceleration Response Spectrum of Seismic Waves

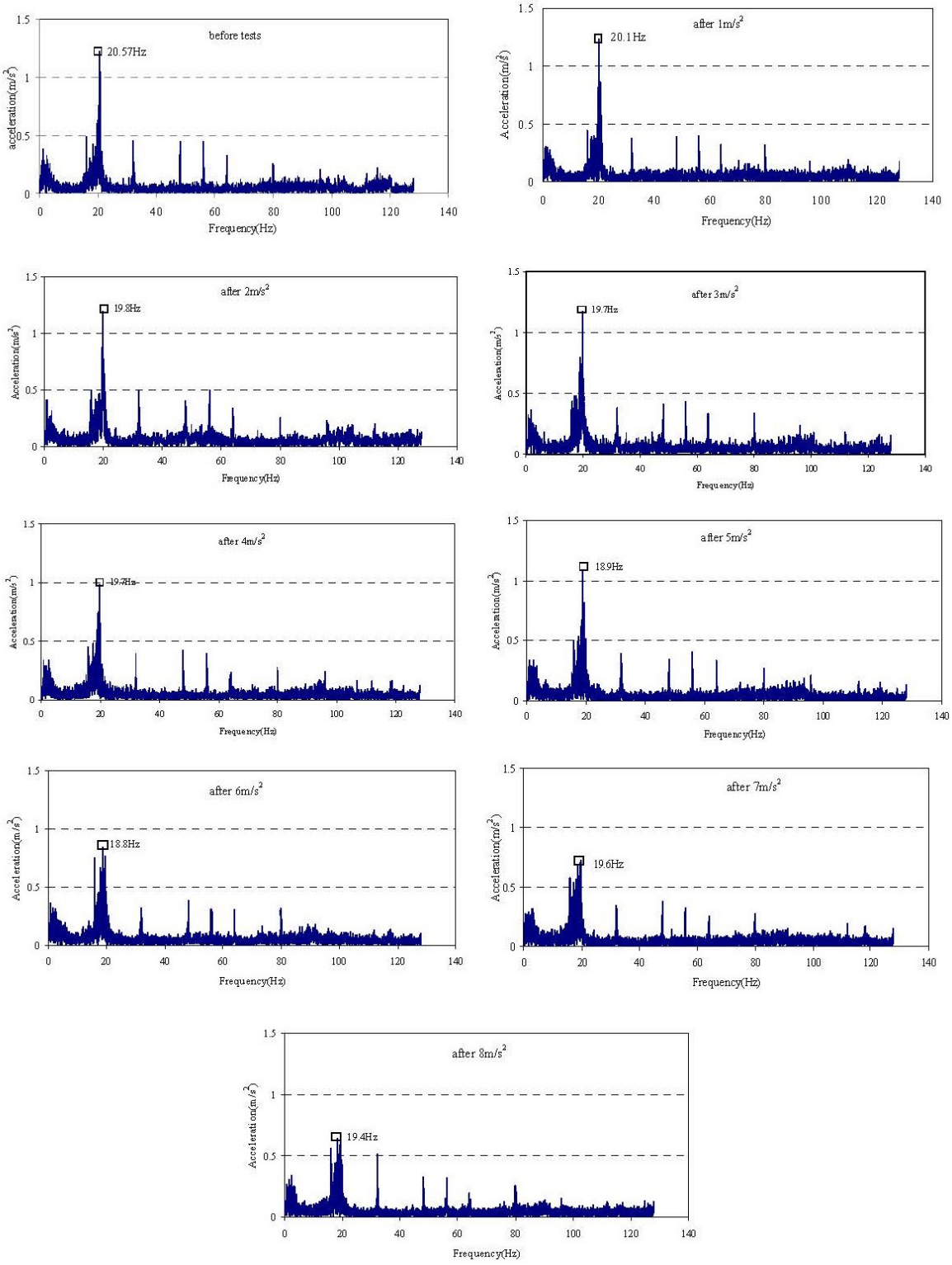

Figure 7. Natural Frequency of Post D

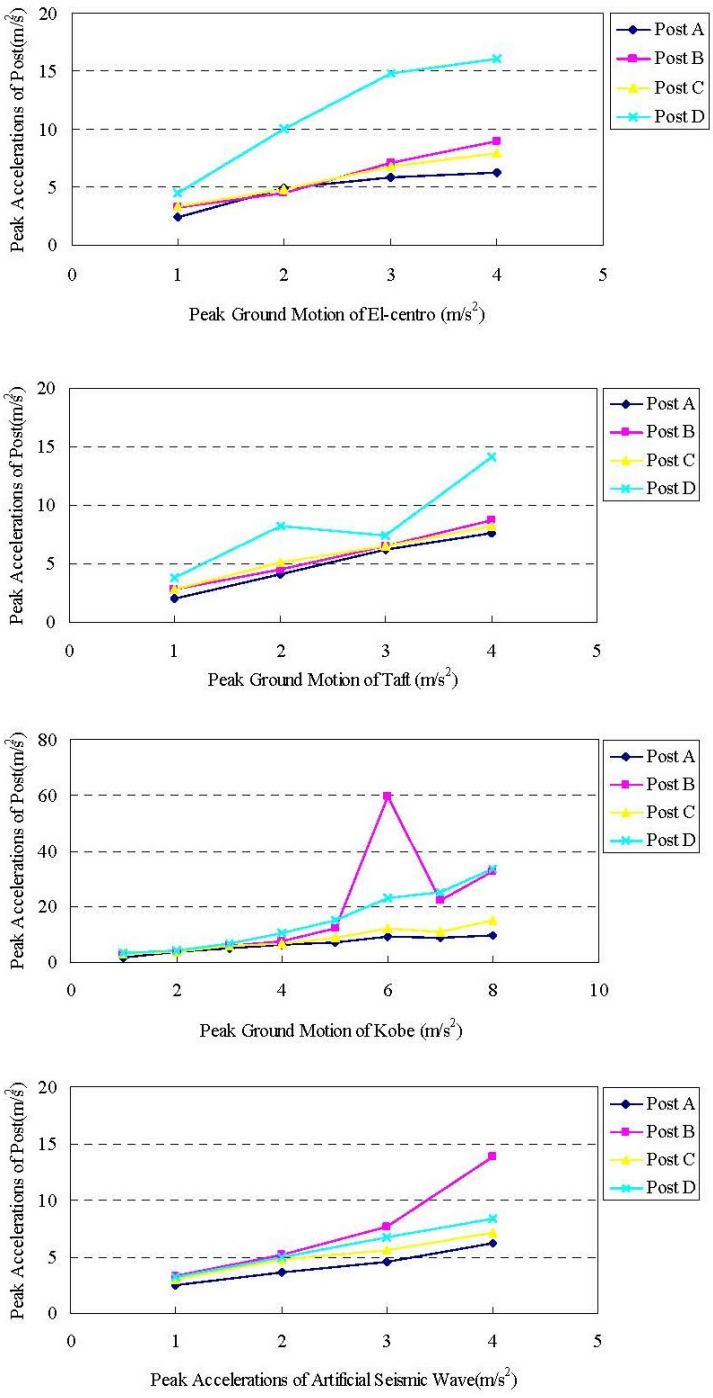

Figure 8. Peak Accelerations of Post form Seismic Tests

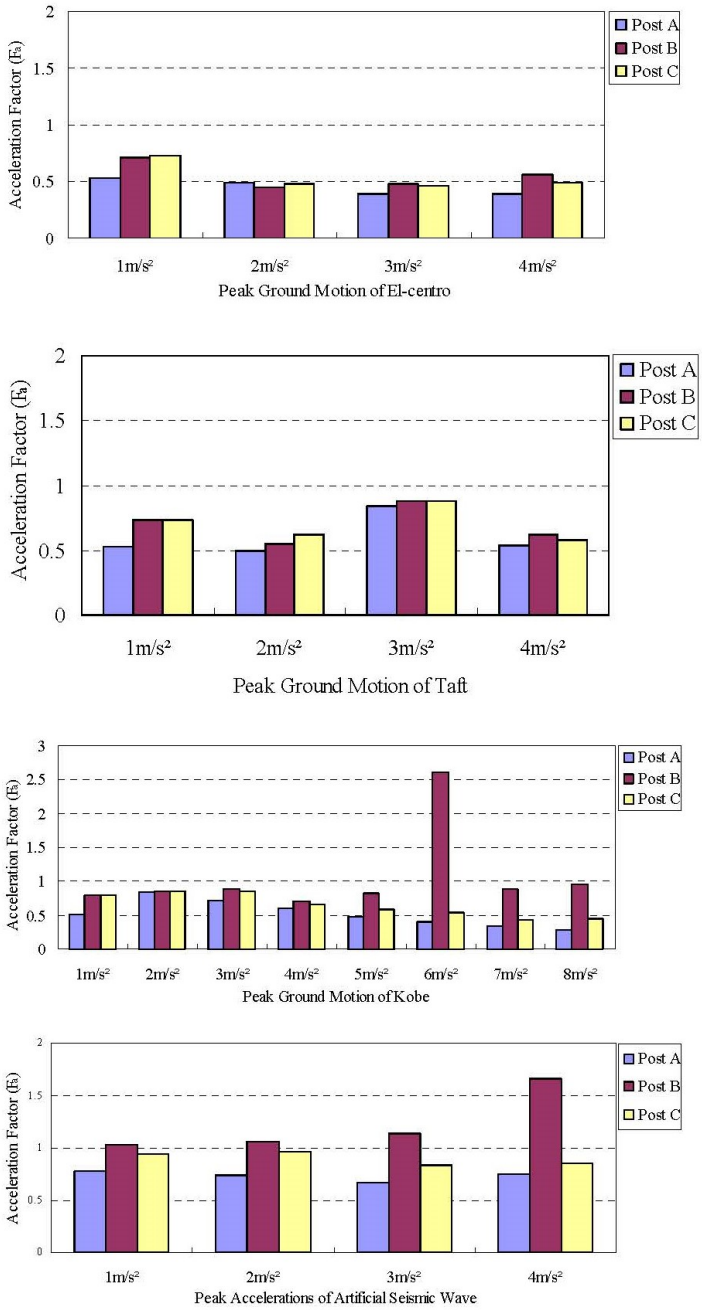

Figure 9. Accelerations Factor form Seismic Tests

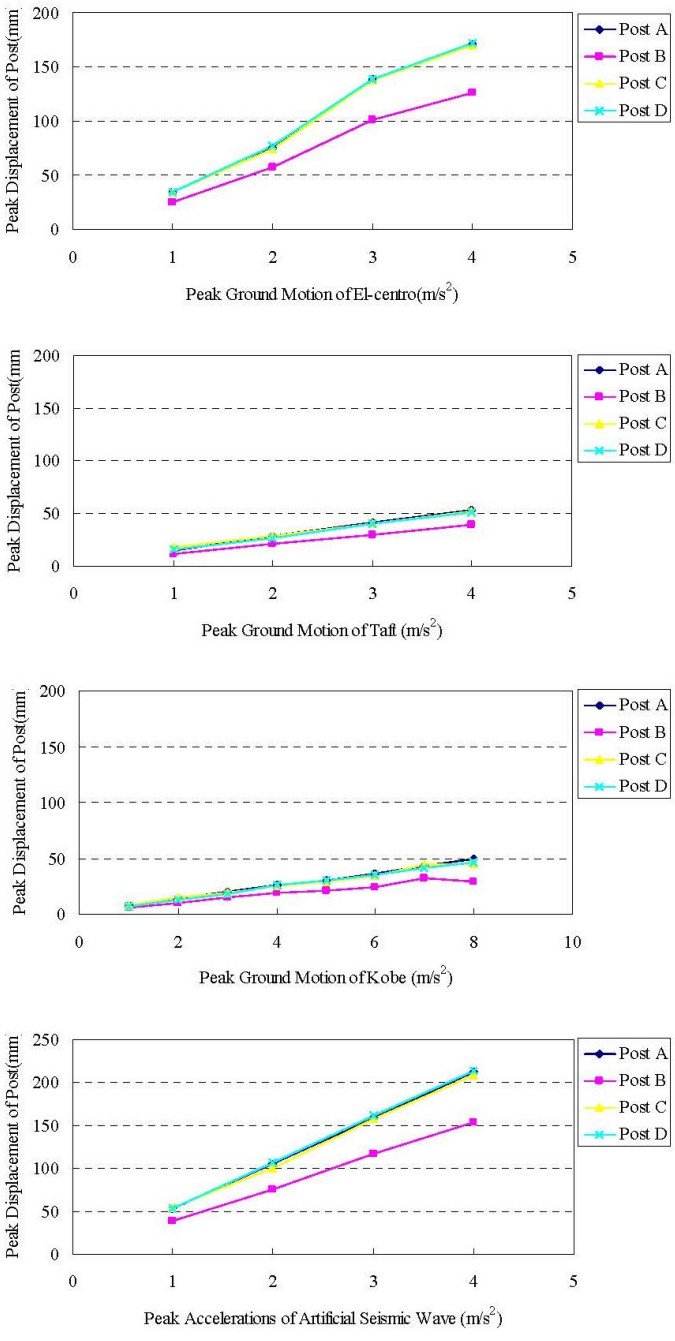

Figure 10. Peak Displacements of Post form Seismic Tests

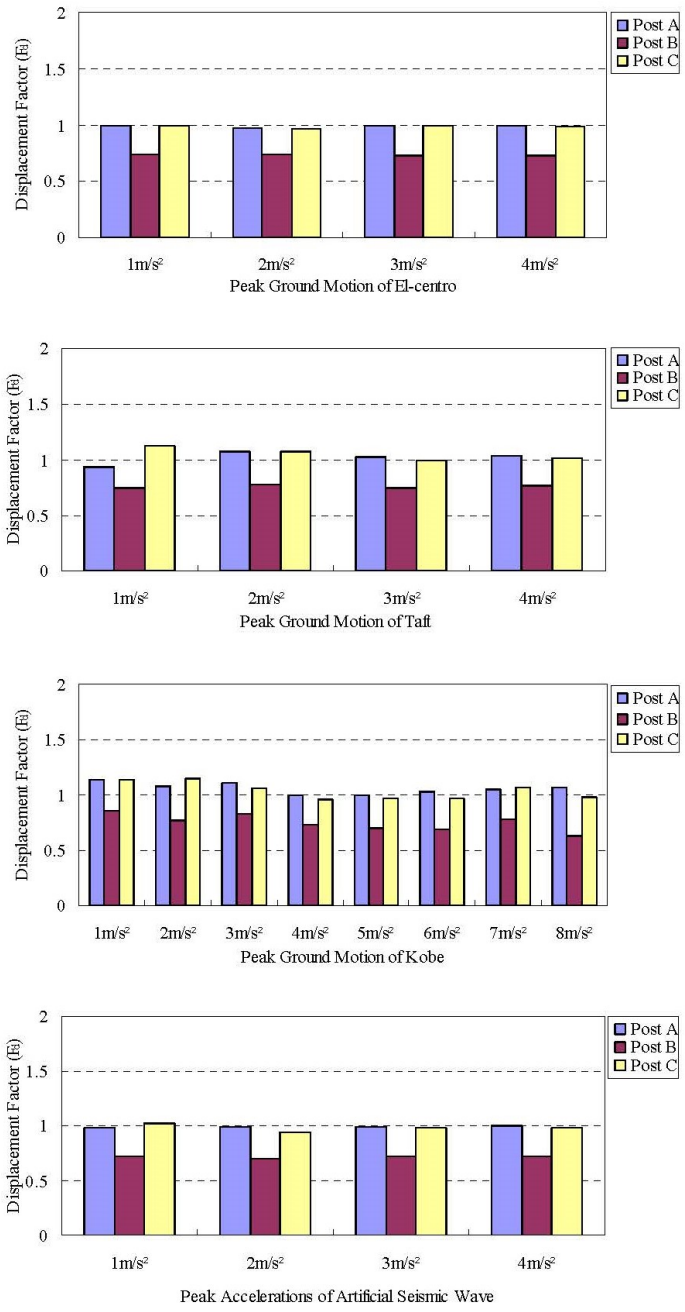

Figure 11. Displacements Factor form Seismic Tests

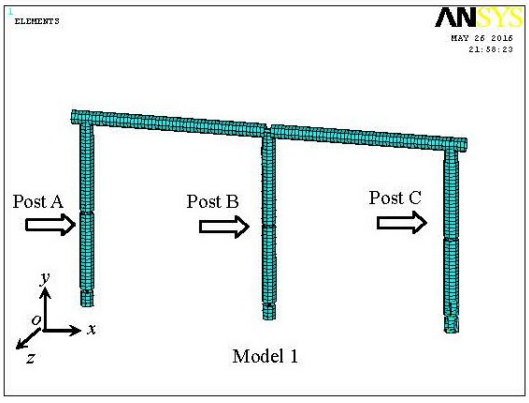

Figure 12. Finite Element Models for Test Structure

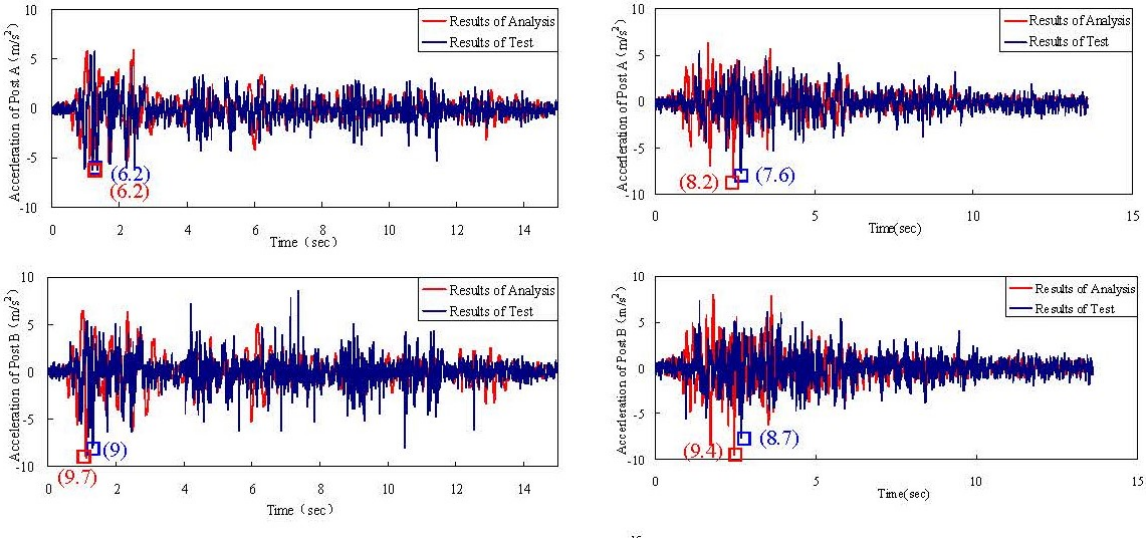

Figure 13. Accelerations-time of Post form Tests and Analysis

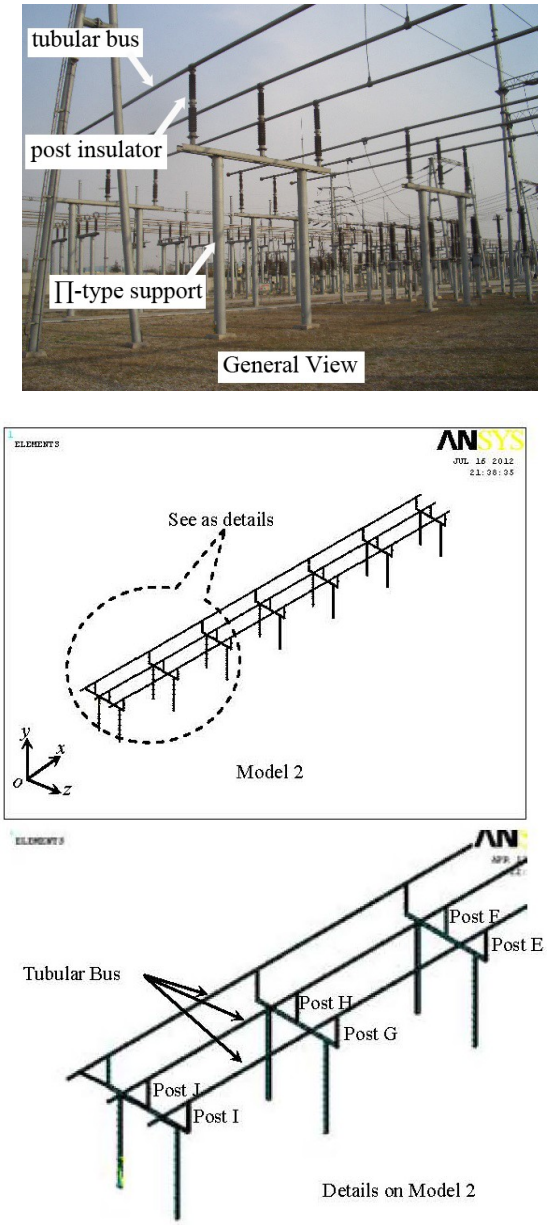

Figure 14. Finite Element Models for Supported Tubular Bus Structure

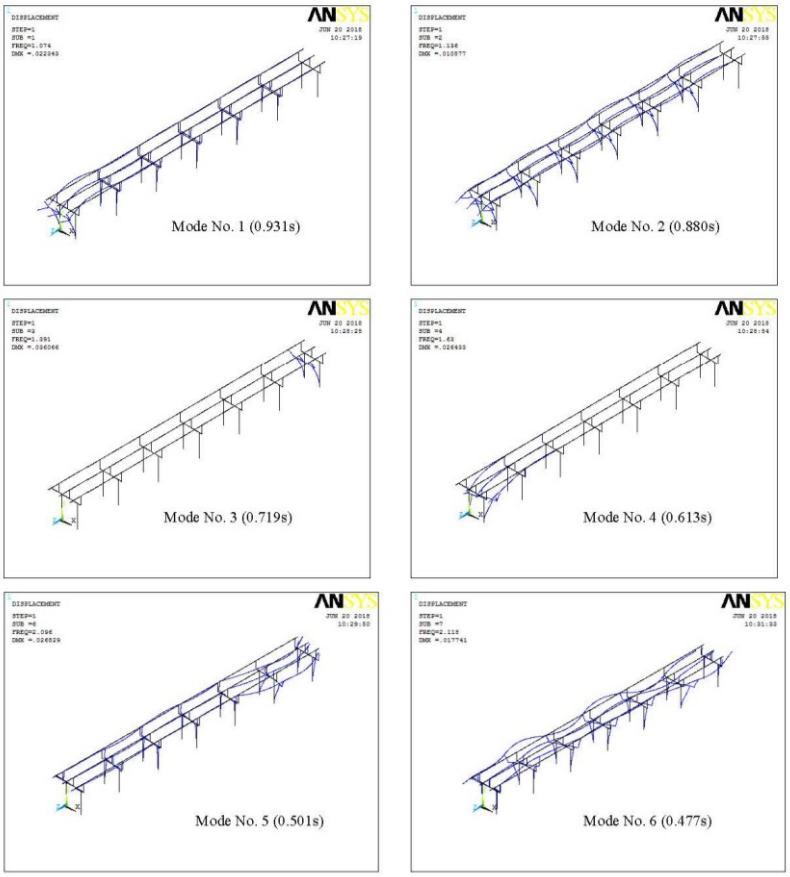

Figure 15. Mode shapes of the Model 2